Exp Fluids (2012) 52:511–517
DOI 10.1007/s00348-011-1241-9

RESEARCH ARTICLE

On the stabilization of leading-edge vortices with spanwise flow

Heather R. Beem · David E. Rival · Michael S. Triantafyllou

Received: 20 June 2011 / Revised: 17 November 2011 / Accepted: 23 November 2011 / Published online: 3 December 2011

Abstract The influence of spanwise flow on the development and stabilization of leading-edge vortices (LEVs) on a foil (without rotational acceleration) has been investigated. The plunging swept wing/fin geometry used in this study, characteristic of fish-like tails, has been found to be insufficient in the stabilization of LEVs. Direct force measurements and visualizations, including Particle Image Velocimetry and lead precipitation, show that despite the presence of a strong spanwise flow at higher sweepback angles, the vortex breaks off and convects downstream at the same relative time as found for low sweepback angles, which experience little spanwise contribution. Although the LEV stabilization is insensitive to bulk spanwise flow, the LEV and tip vortex have been observed to maintain a stronger connection with one another at higher sweepback angles. This result implies that despite similar forces developing for low and high sweepback angles alike, the resulting vortex-wake topologies can vary significantly from one another.

1 Introduction

Depending on the orientation and spatial-temporal scales of an unsteady maneuver or gust, it is not uncommon for the angle of attack of lifting bodies to rapidly vary and thus experience a dynamic-stall event, as described by McCroskey (1982). During such an event, the boundary-layer separation moves rapidly forward to the leading edge, at which point the bulk vortex dynamics are typically found to be less sensitive to Reynolds number; see Ol et al. (2009). In general, this dynamic-stall process leads to the formation of large separated vortical structures, e.g., leading-edge vortices (LEVs) around the lifting surface, thus increasing the loadings substantially. Since the pioneering work by Ellington et al. (1996) on LEV formation in insect flight, a great deal of speculation has developed regarding the specifics of the three-dimensional dynamic-stall process. Here, some of the immediate questions that arise are as follows: What is the time scale associated with the variation in tip-vortex circulation during a rapid change in lift? In such unsteady cases, do the leading-edge and tip vortices vary proportionally in strength to one another? This study presents the basic vortex topology, which should be used to guide future experiments in answering these questions.

When observing efficient aquatic locomotion in nature, for example in the propulsion of oscillating tail fins outlined by Triantafyllou et al. (2000), a swept planform is found to be the most prevalent shape. However, the specific fluid-dynamic role of this planform during oscillatory motions has yet to be properly investigated. Under steady conditions, the effect of sweepback on lift enhancement through leading-edge vortex (LEV) stabilization is well understood, particularly in the context of delta-wing aircraft, as discussed by Polhamus (1971). With increasing degrees of sweepback, one finds a proportionally stronger spanwise flow drawing vorticity away from the leading edge, which in turn is sufficient to maintain LEV attachment.

H. R. Beem · D. E. Rival · M. S. Triantafyllou
Department of Mechanical Engineering, Massachusetts Institute of Technology, 77 Massachusetts Avenue, Cambridge, MA 02139, USA

D. E. Rival (✉)
Department of Mechanical and Manufacturing Engineering, University of Calgary, 2500 University Dr NW, Calgary, AB T2N 1N4, Canada
e-mail: derival@ucalgary.ca

When considering the possibility of spanwise vortex stabilization in natural flyers, Ellington et al. (1996) were the first to observe this phenomenon for the case of a flapping model-hawkmoth wing (Re $\simeq$ 100). They postulated that spanwise flow through the vortex core, causing a conical spiral vortex, was responsible for the redirection of momentum toward the wing tip. This would then allow for the LEV circulation to remain sufficiently small for attachment, similar to the quasi-steady stabilization experienced in the delta-wing LEV arrangement. Not long after Ellington's study, Birch and Dickinson (2001) observed the stable LEV attachment on a fruit-fly wing (Re $\simeq$ 115) and proposed that this stabilization was instead due to the downwash induced by the tip vortex, thus reducing the effective angle of attack. More recently, Lentink and Dickinson (2009) have shown that for a steadily translating fruit-fly wing, neither sweep nor tip effects alone provide stabilization. However, for a continuously rotating model, the LEV can be stabilized when centripetal and Coriolis accelerations play a dominant role. These studies were performed in the Reynolds number range of $100 \leq \mathrm{Re} \leq 15{,}000$.

Other studies including those performed by Parker et al. (2007), Buchholz and Smits (2008), Kim and Gharib (2010) and Suryadi et al. (2010) have considered the unsteady separation behavior on dynamic, very low-aspect ratio planforms. These studies have identified the influence of the wing-tip vortex and its downwash on the development of the LEV, where a reduction or even complete elimination of the local separation can be observed. However, due to very low-aspect ratios used in these experiments, where tip-to-tip aspect ratios were typically on the order of 2, the issue of LEV stabilization could not be addressed directly since tip effects dominated the flowfield. The most recent set of experiments, from which this current study has been inspired, was performed by Jones and Babinsky (2011). In these studies a 'waving-wing' experiment replicated various levels of spanwise flow by impulsively rotating a finite-aspect ratio wing. It was found that regardless of Reynolds number no LEV stabilization was present despite the strong Coriolis and centripetal accelerations induced by rotation.

This study simplifies the investigation of spanwise flow on LEV stabilization by eliminating geometric and kinematic factors that could contribute to the vortex dynamics at hand. In isolation, the sweepback parameter generates a spanwise flow that should force vorticity toward the tip and allow for a greater stabilization of the LEV during rapid changes in incidence. In this way, the effect of spanwise flow on vortex formation on a high-aspect ratio wing can be isolated without the complication of other competing accelerations due to Coriolis forces and centripetal forces.

2 Background

Consider the vorticity equation for an incompressible, barotropic fluid with conservative body forces:

$$\frac{\partial \boldsymbol{\omega}}{\partial t} + (\mathbf{v}\cdot\nabla)\boldsymbol{\omega} = (\boldsymbol{\omega}\cdot\nabla)\mathbf{v} + \nabla\times\left(\frac{\nabla\cdot\bar{\bar{\tau}}}{\rho}\right), \tag{1}$$

where the terms on the right-hand side of the equation represent the stretching/tilting of vorticity due to velocity gradients and the diffusion of vorticity due to viscous effects, respectively. The latter will be neglected here based on the argument that the Reynolds number is sufficiently large and that the time scales associated with the LEV evolution are much more rapid than those associated with vortex diffusion.

To further simplify, one can approximate the LEV as a concentrated vortex line running along the suction surface parallel with the span of the wing. This vortex line will theoretically link up to the tip vortex so as to satisfy the Helmholtz vortex laws. We will now designate a cartesian coordinate system aligned with the vortex line such that x runs in the chordwise direction, y is normal to the wing and z is in the direction of the tip, as shown in Fig. 1. Considering a sectional slice through the LEV well away from the tip region, all gradients of velocity in the z-direction are assumed to be zero:

$$\frac{\partial}{\partial z} \approx 0 \tag{2}$$

such that all components of vortex stretching/tilting tend to zero. These terms would only be present for a root-flapping wing where strong spanwise velocity (and pressure) gradients are present due to increasingly higher accelerations away from the root. This leaves a balance between vorticity production and advection terms, such that:

$$\frac{\partial \omega_z}{\partial t} + u\frac{\partial \omega_z}{\partial x} + v\frac{\partial \omega_z}{\partial y} + w\frac{\partial \omega_z}{\partial z} = 0 \tag{3}$$

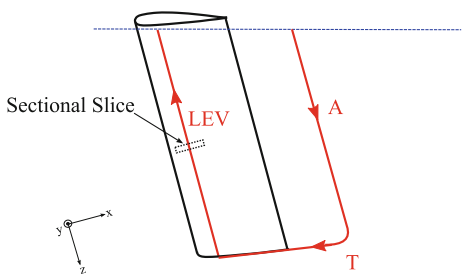

Fig. 1 Schematic depicting a hypothetical vortex topology at early stages of formation, where the LEV is connected with the tip vortex (T) as well as the starting vortex (*A*). If one considers a sectional slice through the LEV away from the tip, and assumes a coordinate system aligned with the span, certain simplifications to the vortex dynamics can be made. Note the arrows show the rotational direction of the vortex assuming a right-hand-rule convention

Therefore, one can postulate that for larger sweepback configurations, an equilibrium state should be attainable so long as the vorticity produced at the leading-edge shear layer is rapidly redistributed and advected away toward the tip. This should serve to drain the vorticity away from the LEV so as to keep it at a manageable size and therefore attached to the wing. As one approaches the wing tip, it can be argued that vortex stretching/tilting will also play an important role in the redistribution of vorticity but this will not be considered for the present. In the current study, an initial investigation to identify the potential stabilization process of a high-aspect ratio LEV has been performed. The following outlines the experimental techniques used to characterize the vortex development and topology as well as its subsequent detachment from the wing.

3 Experimental setup

LEVs were generated on a NACA 0012 wing with rectangular planform. The wing was plunged laterally in a single sideward motion at a geometric angle of $\alpha = 0°$ while towing steadily down the length of the water tank; see Fig. 2. The wing chord had dimensions of $c = 70$ mm with a semi-span of $s = 420$ mm. The wing pierced the free surface to ensure symmetry at this location. Since the motion was relatively slow, no significant free-surface effects are expected here. The plunge motion was modeled as one half the wavelength of a sinusoidal motion corresponding to a Strouhal number of $\mathrm{St} = fd/U = 0.3$, where f is the frequency of the motion and the towing speed was set to $U = 0.2$ m/s ($\mathrm{Re} = 14{,}000$). The characteristic wake width was $d = 140$ mm, chosen as twice that of the lateral motion amplitude and wing chord ($d = 2h_o = 2c$), where the motion is described as:

$$h(t) = h_o \cos(2\pi ft) \tag{4}$$

Although the wing moves steadily forward through the entire run, the effective angle of attack increases to a peak ($\alpha_{\mathrm{eff,max}} = \tan^{-1}(2h_0/U) = 35°$) by the middle of the lateral motion $h(t)$ and then drops back to zero at the end of the lateral motion. The lateral motion was carried out using a single linear motor and was repeated for a range of low and high sweepback angles ($0° \leq \Lambda \leq 45°$).

Direct force measurements were acquired using an ATI Gamma six-axis load cell. A National Instruments USB-6218 data acquisition system was used to collect the amplified sensor output at 1,000 Hz. Figure 3 shows the general positioning of the load cell, drive system and camera. The data were filtered using a Chebychev filter and were ensembled-averaged over ten individual runs. Inertial forces were less than 10% of the total force and were removed by measuring the model's mass and estimating acceleration during the lateral motion. The remaining hydrodynamic force includes the added mass and is the component reported in this study. Values for lift coefficient (normal to the mean flow direction) were calculated using the physical chord (c) and the effective span (s'), where $s' = s \times cos(\Lambda)$. The error was found by calculating the percent difference between data from the individual runs and the ensemble averaged value shown in the plot. It was calculated to have a maximum value of 8%.

Visualizations using Particle Image Velocimetry (PIV) were performed at sweepback angles ($\Lambda = 15°$) and ($\Lambda = 45°$) at both inboard and outboard locations corresponding to 75%-span and 95%-span locations. The spanwise location is defined here as the ratio of the normal distance from the free surface to the plane of interest (d_1) over the total distance to the tip ($s' = d_1 + d_2$). Refer to Fig. 4 for a clear representation of the PIV plane definition. A Nd:YLF laser ($\lambda = 527$ nm) was synchronized with a high-speed camera at a frequency of 600 Hz in single-frame mode, which was towed with the wing, as shown in Fig. 4. Velocity vector fields were calculated using an adaptive-correlation starting with 128 × 128 pixel interrogation windows and then 64 × 64 pixel interrogation windows, both at 50% overlap. Finally, light vector

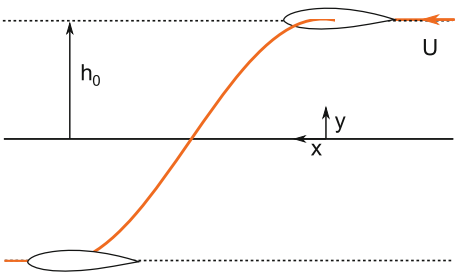

Fig. 2 Schematic depicting the lateral motion, where h_o is the amplitude and U is the towing velocity

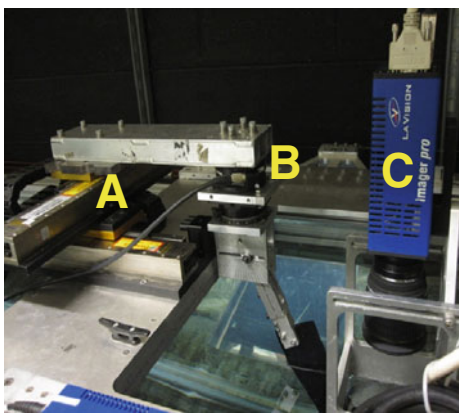

Fig. 3 Experimental setup with linear motor for lateral motion (*A*), 6-component load cell with sweep-angle adjustment below (*B*) and moving PIV camera (*C*)

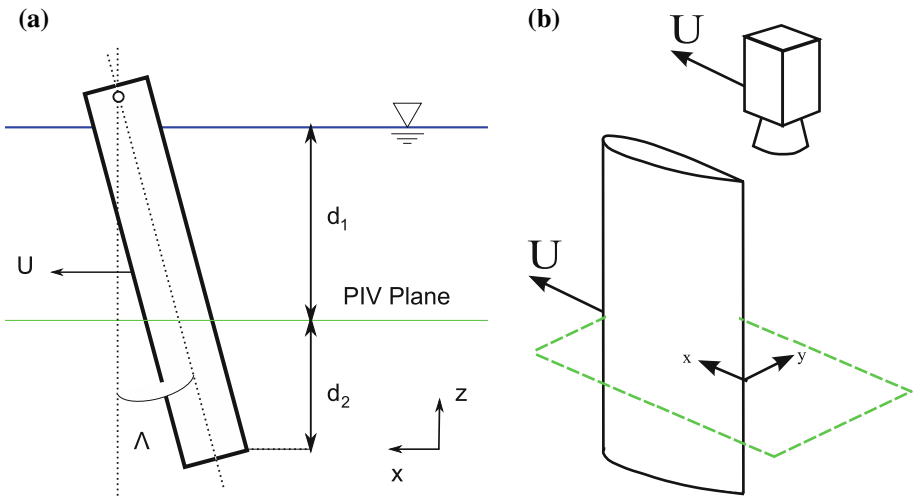

Fig. 4 Schematic depicting **a** the parameter space for the sweepback experiments and **b** the relative position of the moving camera/wing system. The towing velocity is U, the sweepback angle is Λ, and the ratio $d_1/(d_1 + d_2)$ defines the spanwise position of the PIV plane

smoothing was carried out using a standard 3×3 moving filter. The accuracy of the vector fields was estimated to lie within 2% of the towing speed for all cases. Subsequently, the calculation of vorticity could be estimated to have an uncertainty of $\omega c/U = \pm 0.1$.

In order to gain a global view of the vortex structures, lead precipitation was used for flow visualization. This technique uses an electrolytic reaction to produce lead flakes that get caught in the local boundary or shear layers. A 10 mm wide strip of lead tape was placed on the suction side of the foil, along the leading edge. On the opposite side, just aft of the leading edge, a copper tape of similar size was placed along the span to act as a cathode. A differential voltage was held across these two strips (40 V) and table salt was added to the water tank to complete the electrical path. The same laser as for the PIV measurements was also used to illuminate the lead precipitate. Instead of a thin horizontal sheet, a volume of laser light was created by sending a loosely focused laser beam through a cylinder lens. This expanded the light into a thick vertical sheet used to illuminate the entire region of interest. Images were recorded using a Canon EOS Rebel T2i camera with hi-definition video at 30 frames per second, providing a qualitative description of the three-dimensional vortex system. The same technique was repeated with the lead and copper strips flipped to opposite sides of the foil in order to visualize the pressure side of the foil. Note that due to ease of experimental setup, the direction of lateral motion was flipped from that shown in Fig. 2, i.e., the foil in the lead precipitation visualizations started at $-h_0$ and ended at h_0.

4 Results

Lift coefficients corresponding to the hydrodynamic lift forces on the foil are shown in Fig. 5. The start and end of the translatory motion is designated by $t/T = 0$ and $t/T = 1$, respectively. All sweepback angles tested

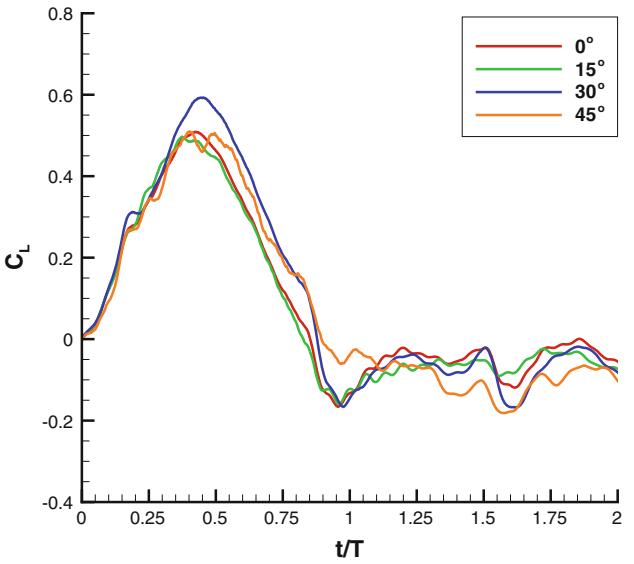

Fig. 5 Time-dependent lift coefficient for various sweepback angles, where $t/T = 0$ and $t/T = 1$ represent the beginning and end of the lateral motion, respectively. Variation between the four lines lies within the error band

($\Lambda = 0°$, 15°, 30° and 45°) show similar variations in lift, which suggests that the LEV is rapidly convected away soon after the mid-stroke position ($t/T = 0.5$) for all cases. The $\Lambda = 30°$ sweepback angle demonstrates a slightly higher peak in lift, and the $\Lambda = 45°$ sweepback angle demonstrates a slightly more sustained value, suggesting a minor degree of LEV stabilization, but not by an amount larger than the possible errors in the force measurements.

In order to track the evolution of the LEV during the lateral motion, PIV measurements were performed for two sweepback cases ($\Lambda = 15°$ and 45°) representing cases of mild and strong spanwise velocity components, respectively. Figures 6 and 7 display contours of non-dimensional vorticity associated with inboard (75%-span) and

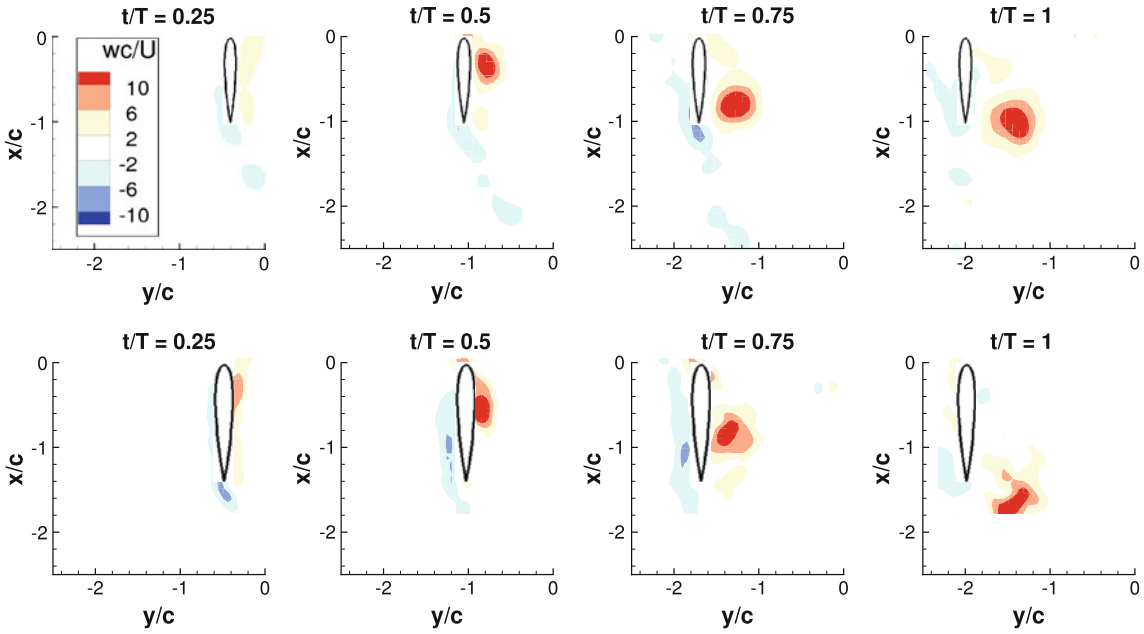

Fig. 6 Cross-section of the LEV evolution at the 75%-span position through four time steps in the plunge cycle for $\Lambda = 15^\circ$ (*top row*) and $\Lambda = 45^\circ$ (*bottom row*). Note that the axes are non-dimensionalized with the chord ($c = 70$ mm)

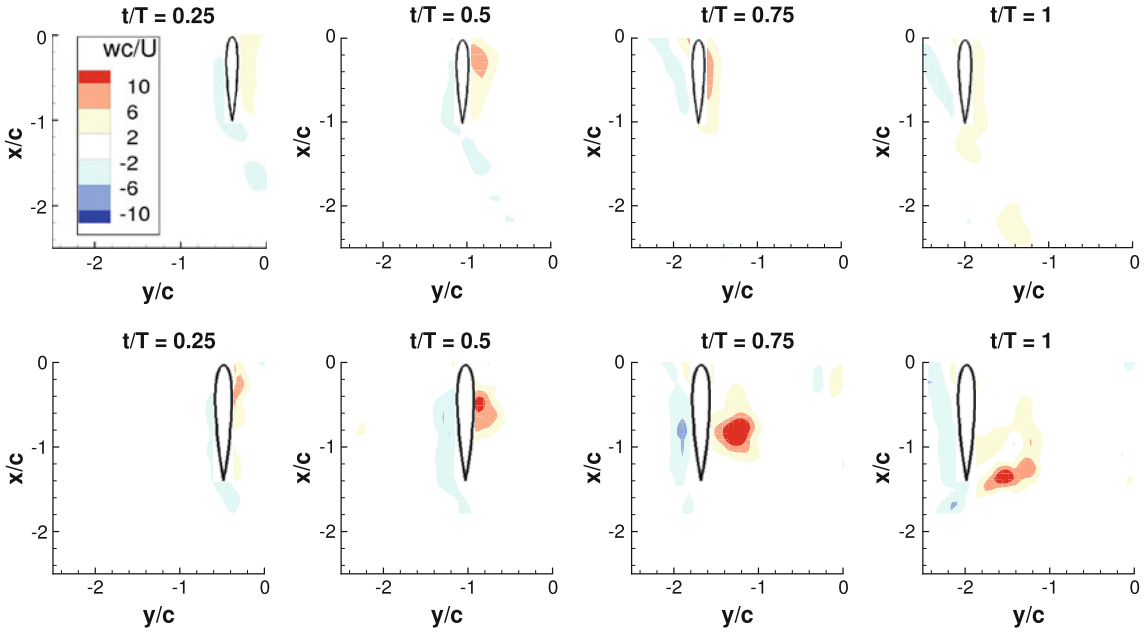

Fig. 7 Cross-section of the LEV evolution at the 95%-span position through four time steps in the plunge cycle for $\Lambda = 15^\circ$ (*top row*) and $\Lambda = 45^\circ$ (*bottom row*). Note that the axes are non-dimensionalized with the chord ($c = 70$ mm)

outboard (95%-span) measurement planes during distinct steps of the motion. Refer to the definition of spanwise location as shown in Fig. 4. The leading edge of the wing starts in the upper-right corner of the frame ($x/c = y/c = 0$) at the beginning of the motion and traverses to the left to its end position ($x/c = 0$, $y/c = -2$). By the halfway point in the translatory motion ($t/T = 0.5$), the formation of a coherent LEV structure is evident for both sweepback angles at the inboard position; see Fig. 6. Here, the LEV is found to subsequently grow in size and strength, while moving downstream in the chordwise direction. In Fig. 7, at the outboard measurement plane, a similar behavior is observed for the $\Lambda = 45^\circ$ case. In stark contrast, however, the out-of-plane vorticity for the $\Lambda = 15^\circ$ case is weak,

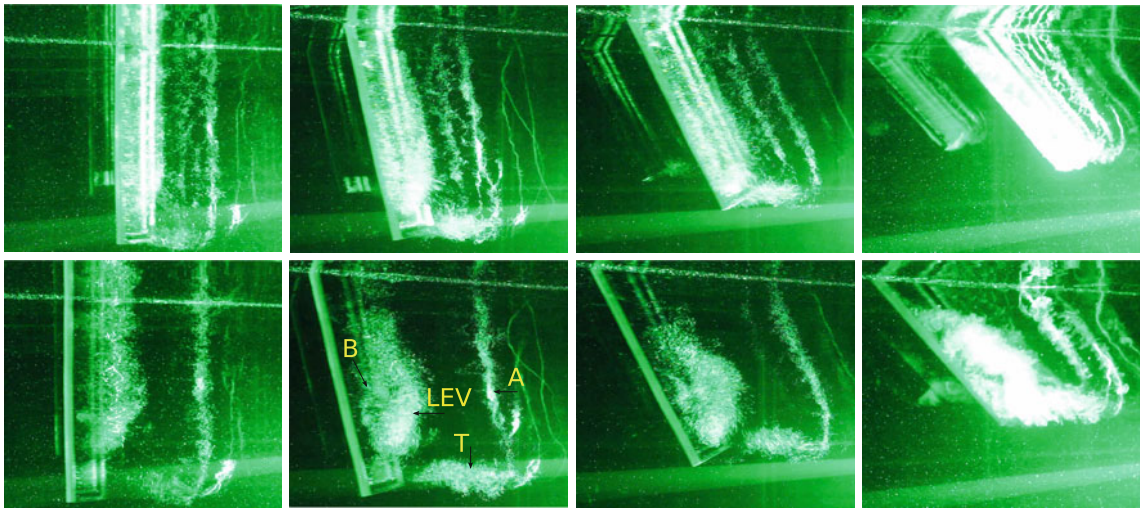

Fig. 8 Lead precipitation visualizations on wing suction side during second half of lateral motion; from *left* to *right* sweepback angles of $\Lambda = 0°$, 15°, 30° and 45° at $t/T = 0.75$ (*top row*) and $t/T = 1$ (*bottom row*). *A*, *B*, *T* and *LEV* represent the starting, stopping, tip and LEV vortices in the wake, respectively. As sweepback angle goes up, connection between vortex structures increases

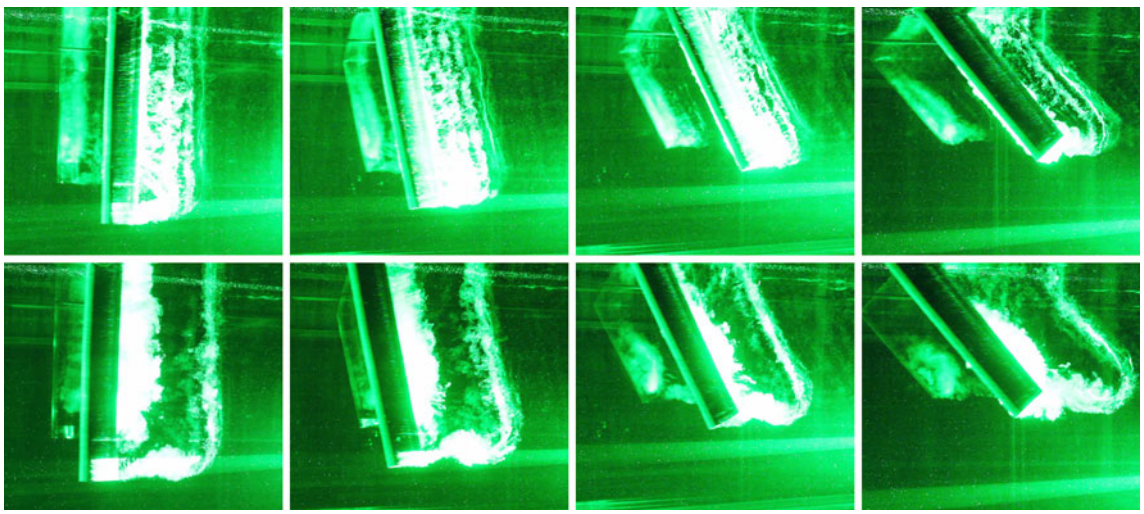

Fig. 9 Lead precipitation visualizations on wing pressure side during second half of lateral motion; from *left* to *right* sweepback angles of $\Lambda = 0°$, 15°, 30° and 45° at $t/T = 0.75$ (*top row*) and $t/T = 1$ (*bottom row*). Note that a reflection off of the tank's back wall can be seen just to the *left* of the actual foil

suggesting that the LEV diffuses or breaks apart near the wing tip. Despite this fundamental difference in vortex topology in the tip region, clearly the lack of LEV stabilization is common to both sweepback angles.

Now to properly ascertain the global vortex topology for both low and high sweepback cases, lead precipitation visualizations were performed at two later time steps ($t/T = 0.75$, $t/T = 1$) on both suction and pressure sides of the wing, shown in Figs. 8 and 9, respectively. The topology was found to consist of four main structures: LEV, tip vortex, start vortex, and stop vortex. The latter two are a result of the beginning and end of the lateral motion, respectively. For the low sweepback angles, $\Lambda = 0°$ and 15°, the LEV and tip vortices are not clearly connected; in particular see bottom rows ($t/T = 1$) in Figs. 8 and 9, where there appears to be a gap region between the two. This is due to downwash, which is flow over the tip toward the pressure side, preventing vortex structure connection within the tip region. The general vortex topology is depicted in Fig. 10, which shows that the tip and start vortex are connected together, but are not connected to the LEV/stop vortex system. However, for higher sweepback angles, $\Lambda = 30°$ and 45°, the LEV wraps strongly together with the tip vortex; again refer to bottom rows ($t/T = 1$) in Figs. 8 and 9. As sketched in Fig. 11, a stronger connection between LEV/stop vortices with the

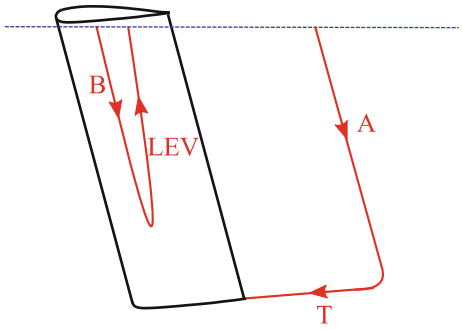

Fig. 10 Resulting vortex topology at $t/T = 1$ for low sweepback cases (here $\Lambda = 15°$), where *A*, *B*, *T* and *LEV* represent the vortices as described in Fig. 9. Note the *arrow* shows the rotational direction of the vortex assuming a right-hand-rule convention

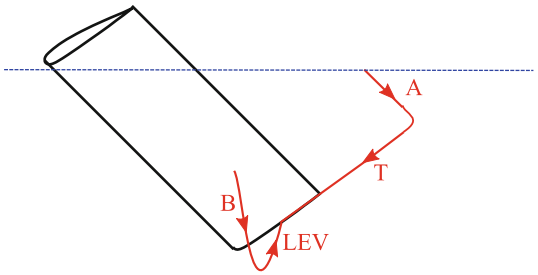

Fig. 11 Resulting vortex topology at $t/T = 1$ for high sweepback cases (here $\Lambda = 45°$), where *A*, *B*, *T* and *LEV* represent the vortices as described in Fig. 9. Note the *arrow* shows the rotational direction of the vortex assuming a right-hand-rule convention

tip/start vortices is clearly observed. The wake in these higher sweepback angle cases then resembles the start of a typical vortex-ladder such as that shown in Henningsson et al. (2008). The full implications of the vortex topologies are unknown, however their basic characteristics and their clear differences should be used to inform future studies.

5 Conclusions

In this study, the influence of spanwise flow, which is directly proportional to sweepback, on LEV stabilization has been examined for a rapidly translating wing. LEV stabilization has been found to be absent for all degrees of spanwise flow tested here. This implies that the sweepback geometry typical of fish tails serves some other function. It is possible that some specific combination of spanwise flow, three-dimensional kinematics, rotation, and/or flexibility would provide a degree of LEV stabilization.

The primary finding of this study is in agreement with the recent work of Jones and Babinsky (2011) for a sweeping (rotating) wing and has been evidenced primarily by direct, time-resolved force measurements. PIV and lead precipitation visualizations further support this result and also show that despite the lack of LEV stabilization, significant differences in the wake topology occur for these varying cases. At low sweepback angles, the induced flow from the tip vortex has a downwash effect, which prevents flow separation near the tip. The LEV and tip vortex, therefore, do not demonstrate a clear connection with one another. In contrast to this gap region between the two vortex structures at low sweepback angles, high sweepback angles show increased connection and therefore form more pronounced vortex-ladder type wakes.

Acknowledgments We would like to thank J. Dahl for his advice regarding the force measurements and lead precipitation visualizations. Also the authors are grateful for the insight and encouragement provided by H. Babinsky on this topic.

References

Birch JM, Dickinson MH (2001) Spanwise flow and the attachment of the leading-edge vortex on insect wings. Nature 412:729–733

Buchholz JHJ., Smits AJ (2008) The wake structure and thrust performance of a rigid low-aspect-ratio pitching panel. J Fluid Mech 603:331–365

Ellington CP, van den Berg C, Willmott AP, Thomas ALR (1996) Leading-edge vortices in insect flight. Nature 384:626–630

Henningsson P, Spedding GR, Hedenstrom A (2008) Vortex wake and flight kinematics of a swift in cruising flight in a wind tunnel. J Exp Biol 211:717–730

Jones AR, Babinsky H (2011) Reynolds number effects on leading-edge vortex development on a waving wing. Exp Fluids 51(1):197–210. doi:10.1007/s00348-010-1037-3

Kim D, Gharib M (2010) Experimental study of three-dimensional vortex structures in translating and rotating plates. Exp Fluids 49(1):329–339

Lentink D, Dickinson MH (2009) Rotational accelerations stabilize leading edge vortices on revolving fly wings. J Exp Biol 212:2705–2719

McCroskey WJ (1982) Unsteady airfoils. Annu Rev Fluid Mech 14:285–311

Parker K, von Ellenrieder KD, Soria J (2007) Morphology of the forced oscillatory flow past a finite-span wing at low Reynolds number. J Fluid Mech 571:327–357

Polhamus EC (1971) Predictions of vortex-lift characteristics by a leading-edge suction analogy. J Aircraft 8:193–199

Ol MV, Bernal L, Kang C-K, Shyy W (2009) Shallow and deep dynamic stall for flapping low Reynolds number airfoils. Exp Fluids 46(5):883–901

Suryadi A, Ishii T, Obi S (2010) Stereo PIV measurement of a finite, flapping rigid plate in hovering condition. Exp Fluids 49(2):447–460

Triantafyllou MS, Triantafyllou GS, Yue DKP (2000) Hydrodynamics of fishlike swimming. Annu Rev Fluid Mech 32:3353